Biochimica et Biophysica Acta, 1101 (1992) 105–119

BBABIO 43594

The dependence of the degrees of sigmoidicities of fluorescence induction curves in spinach chloroplasts on the duration of actinic pulses in pump-probe experiments

Louisa L. France [a], Nicholas E. Geacintov [a], Jacques Breton [b] and Leonas Valkunas [c]

[a] *Chemistry Department, New York University, New York, NY (USA),* [b] *Service de Biophysique, Departement de Biologie, Centre d'Etudes Nucleaires de Saclay, Gif-sur-Yvette (France) and* [c] *Institute of Physics, Lithuanian Academy of Sciences, Vilnius (Lithuania)*

(Received 9 August 1991)
(Revised manuscript received 6 January 1992)

Key words: Photosystem II; Reaction center; Fluorescence; Chloroplast; Fluorescence induction curve; (Spinach)

Utilizing a pump-probe double flash method, the shapes of the fluorescence induction curves in spinach chloroplasts (0°C), and the induction ratio $R = F_M/F_0$ (F_0 and F_M are the fluorescence yields when all PS II reaction centers are open, and closed, respectively) were studied as a function of: (1) the duration (t_1) of the pump flash, (2) the number of pump flashes, (3) absence or presence of DCMU, and (4) the time interval Δt between the pump and the probe flashes. In the pump-probe technique, an actinic pulse (P_1) of different fluences closes a fraction q of the PS II reaction centers. After a variable time interval Δt a second, weak pulse (P_2), is used to measure the variable fluorescence yield F_v. The shapes of the fluorescence induction curves (F_v vs. the fluence of the P_1 pulse) were analyzed in terms of the standard equation $F_v = (1-p)q/(1-pq)$, where p is a parameter describing the connectivity between different photosynthetic units (Joliot, A. and Joliot, P. (1964) C. R. Acad. Sci. 13, 4622–4625). The shapes of the F_v curves are found to depend only on the width (t_1) of the pump pulses. For $t_1 \lesssim 300$ ps, the curves are exponential in shape with $p = 0.0$ and $R < 2.5$. However, for pulse durations t_1 in the millisecond range, and employing the same probe flash method for measuring the variable fluorescence, the F_v curves assume the same familiar sigmoidal shapes as in the case of conventional steady-state illumination. With t_1 in the microsecond range ($t_1 \approx 0.7$–2 μs), the F_v curves are more nearly exponential than sigmoidal in shape with p values generally around ≈ 0.3 and $R < 3$. For $t_1 \gtrsim 50$ μs, the fluorescence induction curves are sigmoidal in shape and, generally, p values of 0.55–0.60 are observed with $R > 3$. A sequential hit model (Valkunas, L., Geacintov, N.E., France, L. and Breton, J. (1991) Biophys. J. 59, 397–408), in which the PS II reaction centers evolve through different states characterized by differences in fluorescence yields, a process characterized by a dark-time t_1 of ≈ 2–50 μs between two successive hits, can account for these results. This model is consistent with the concept of interunit transfer of excitations. However, the shapes of the fluorescence induction curves cannot provide any information on the value of p within the context of this model.

1. Introduction

The fluorescence intensity of chloroplasts in green plants and green algae depends on the state of the PS II reaction centers [1,2]. The fluorescence intensity varies from a minmum F_0 (reaction centers open) to a maximum value of F_M (all reaction centers closed). The variable (or induced) fluorescence, F_V, is defined as the ratio:

$$F_v = \frac{F - F_0}{F_M - F_0} \quad (1)$$

Fluorescence induction has traditionally been studied using steady-state illumination, on timescales in the millisecond to second range [1,3–5]. Plots of F_V versus time of illumination are sigmoidal in shape, and the induction ratio, $R = F_M/F_0$, lies in the range $3 \leq R \leq 5$.

Correspondence (present address): L.L. France, Plum Island Animal Disease Center, USDA/ARS, P.O. Box 848, Greenport, NH 11944, USA.

(UFS-200, Instruments SA., Metuchen, NJ). A red, high-band-pass filter (> 665 nm, #2-64, Corning, Corning, NY) was placed in front of the slit to eliminate scattered light. The signal was determined by a photodiode array/ optical multichannel analyzer (OMA, Model 1205D, Princeton Applied Research), and processed by an analog-to-digital converter module (Model 1205A, Princeton Applied Research). The diode array system was gated on and off with a time-delayed pulse from a high voltage pulse generator (Model 1211, EG&G Princeton Applied Research, Princeton, NJ). Each data point reported here represents the mean of three experiments, with each experiment representing 100–300 accumulations, unless stated otherwise; the error bars are within the width of the data points, unless explicitly indicated otherwise. In all experiments, the F_0 fluorescence signal (fluorescence yield of dark-adapted chloroplasts, generated by the P_2 flash in the absence of actinic flashes) was recorded throughout the experiment, in order to monitor the stability of the fluorescence of the sample. In quasi-steady-state experiments employing He-Ne laser illumination, the output of the photomultiplier tube was fed directly to a digital oscilloscope system (Model 4203, EG&G Princeton Applied Research).

2.6. Data analysis

The experimentally measured fluorescence induction curves were fitted, in each case, by the sigmoidal fluorescence induction model based on Eqns. 2 and 3, in which p and σ were the unknown parameters; the value of p determines the shape of the fluorescence induction curve, while the values of σI_1 determine its position along the horizontal axis (where I_1 is the fluence of the P_1 pulse). Combining Eqns. 2 and 3, the following expression was generated and used in the fitting procedures:

$$\ln\left\{\frac{pF_V + 1 - p - F_V}{pF_V + 1 - p}\right\} - \frac{pF_V}{(pF_V + 1 - p)(1 - p)} = -\frac{\sigma I_1}{1 - p} \qquad (4)$$

This equation was solved numerically for F_V (Eqn. 1) in terms of I_1, with the best values for p and σ being determined by a non-linear least-squares technique, based on the Marquardt algorithm [19] and adapted from Bevington [20]. The value of p was constrained to be non-negative. The best values for p and σ were determined by minimizing the value of χ^2:

$$\chi^2 = \frac{\sum_{i=1}^{N} [F(I_1, i) - F_{th}(I_1, i)]^2}{\nu} \qquad (5)$$

where N is the number of experimental data points, $F(I_1)$ is the experimentally measured value of F_V at I_1, $F_{th}(I_1)$ is the value of F_V calculated from given values of I_1 from Eqn. 4, and ν is the number of degrees of freedom ($\nu = N - 2$, since the number of floating parameters is 2). The residuals calculated in Eqn. 5 are unweighted, and therefore, the minimum value of χ^2 is expected to approach zero in the ideal case.

The experimental data were normalized to unity at F_0, and the value for F_M (Eqn. 1) was determined by inspection of the experimental data. All experimental data points (fluorescence yield monitored by the probe flash vs. fluence of the actinic pulse, or $F_2(I_1)$ vs. I_1, are plotted so that the corresponding induction ratios, R, are clearly evident from the data plots. It should be noted that the calculated values of p are sensitive to the values of F_M. However, F_M is known to be variable over time, and from sample to sample. We generally observed a small decrease in F_M during the first hour after sample preparation. After this initial decrease, F_M was stable up to $\approx$ 24 h at 0°C.

3. Results

3.1. General considerations

We first consider some of the factors which affect the shapes of the pump-probe fluorescence induction curves. The time delay, Δt, between the actinic and probe flashes must be long enough so that singlet and triplet exciton quenchers [2] created by the pulse P_1, decay prior to the arrival of P_2. If the lifetimes of the excitations are limited by quenchers, the diffusion range of the excitations is expected to be limited, $p \rightarrow 0$, and the fluorescence induction curves are expected to be exponential in shape [21]. Singlet excitations decay within 1 ns, while the lifetimes of the chlorophyll *a* and carotenoid triplets are of the order of 10 ns [22], and ~ 5 μs [23,24], respectively. Therefore, neither singlet nor triplet quenchers are present when the fluorescence yield is probed with the P_2 flashes, 30 μs or more after the actinic flash. However, triplet excited states could, in principle, affect the closing of PS II reaction centers during the actinic flashes of microsecond duration, and thus influence the shapes of fluorescence induction curves measured with the probe flashes. This possibility is discussed in section 4.2 below.

The oxidized state of the primary donor (P^+) of PS II is also an efficient exciton quencher [24–26]; thus Δt must be long enough to allow for the decay of P^+, prior to the arrival of P_2. The time constant for the decay of P^+ after single flashes has been reported to be in the range of 20–35 ns [24,26–28]. However, when trains of laser flashes are used, up to 15% of the P^+ state decays on microsecond time-scales [29]; since, in almost all of our experiments, single actinic flashes were utilized, this effect was neglected. Experimentally, following a 300 ps, 337 nm actinic flash, the maximum probe flash-fluorescence yield, F_2, is observed when

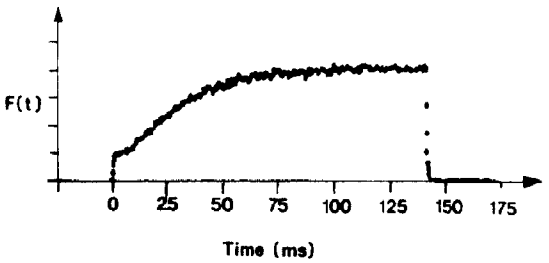

Fig. 2. Fluorescence induction curve obtained under steady-state illumination. Spinach chloroplasts with 10 μM DCMU, 0°C. Excitation source: helium neon laser (fluence rate: $2 \cdot 10^{16}$ photons cm^{-2} s^{-1}. The fluorescence induction ratio, R_{ss}, is 4.0.

$\Delta t \approx 30$ to 50 μs [16], suggesting that quenchers are no longer operative on these time-scales [30].

It is important that q should remain constant until the probe flash P_2 arrives. The upper limit on Δt is determined by the time constant for the re-oxidation of the PS II primary acceptor Q_A^-. In the absence of external inhibitors (e.g., DCMU), re-oxidation of Q_A^- becomes apparent ~ 50–100 μs after a saturating actinic flash.

Due to the constraints imposed by the decay times of quenchers and the lifetime of the reduced form of the primary acceptor, a time delay Δt of 30–100 μs was selected. In the presence of 10 μM DCMU, the time delay was varied up to at least 1 s; the fluorescence yield generated by the P_2 pulse remained constant in this range of Δt values.

3.2. Contrast between submicrosecond actinic flash-induced and steady-state illuminated fluorescence induction curves

The difference in the shapes of the fluorescence induction curves measured under steady-state illumination conditions (Fig. 2), and by the pump-probe technique using single short actinic flashes (Figs. 3A and 3B are quite striking. Fig. 2 shows a conventional steady-state-illuminated fluorescence induction curve, generated by a CW He-Ne laser beam, over a 135 ms period, and in the presence of 10 μM DCMU. The steady-state illumination fluorescence induction ratio, $R_{ss} = F_M/F_o$, was equal to = 4.0 in these experiments. The obvious sigmoidicity and the relatively high value of R_{ss}, are typical of traditional steady-state-illuminated induction curves.

In Fig. 3A, the fluorescence induction curves were measured with a 2 μs probe pulse incident on the sample 100 μs after a 700 ns, 650 nm actinic pump flash (without DCMU); the calculated value of the fluorescence induction ratio, R, which provides the best fit to the data, is 1.73. The solid line represents the best fit of Eqn. 4 to the experimental data points ($p = 0.265$ and $\sigma = 1.55 \cdot 10^{-14}$ cm^2). Sigmoidicity is negligible, and the value of R is lower than in the steady-state illumination case (Fig. 2).

The data in Fig.3B were generated with a 300 ps, 337 nm pump flash, followed by a 2 μs xenon probe flash, with $\Delta t = 30$ μs (no DCMU). The induction ratio is also small ($R = 2.23$). The solid line presents the best fit of Eqn. 4, to the data ($p = 0.0$, and $\sigma = 4.59 \cdot 10^{-15}$ cm^2).

3.3. Comparison of fluorescence induction curves measured by the pump-probe and steady-state illumination techniques

According to Eqns. 2 and 3, the variable fluorescence yield should depend on q in a non-linear manner. The fraction of closed reaction centers depends on the fluence only, and the manner of delivering photons to PS II, either by pulsed or steady-state illumination

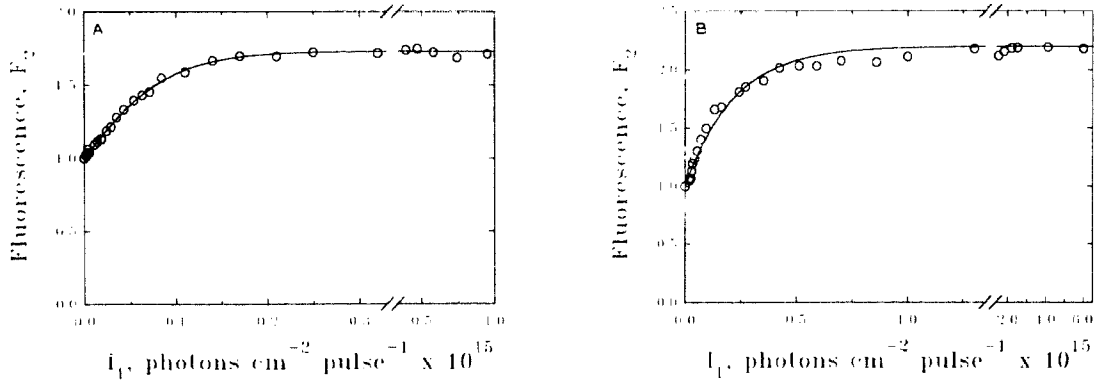

Fig. 3. (A) Variable fluorescence yield ($F_2(O)$ as a function of fluence of the actinic pulse, generated by a 2 μs xenon probe flash, incident on the sample 100 μs after a 700 ns, 650 nm, actinic laser pump flash. The solid line represents the best fit of Eqn. 4 to the experimental data points ($p = 0.265$, $\sigma = 1.55 \cdot 10^{-14}$ cm^2, and $R = F_M/F_o = 1.73$).(B) Variable fluorescence yield ($F_2(O)$) as a function of fluence of the actinic pulse, generated by a 2 μs xenon probe flash incident on the sample 30 μs after a 300 ps, 337 nm, nitrogen laser pump flash. The solid line represents the best fit of Eqn. 4 to the experimental data points ($p = 0.0$, $\sigma = 4.59 \cdot 10^{-15}$ cm^2, $R = 2.2$). The diode array system was used in these experiments for detecting the fluorescence signals.

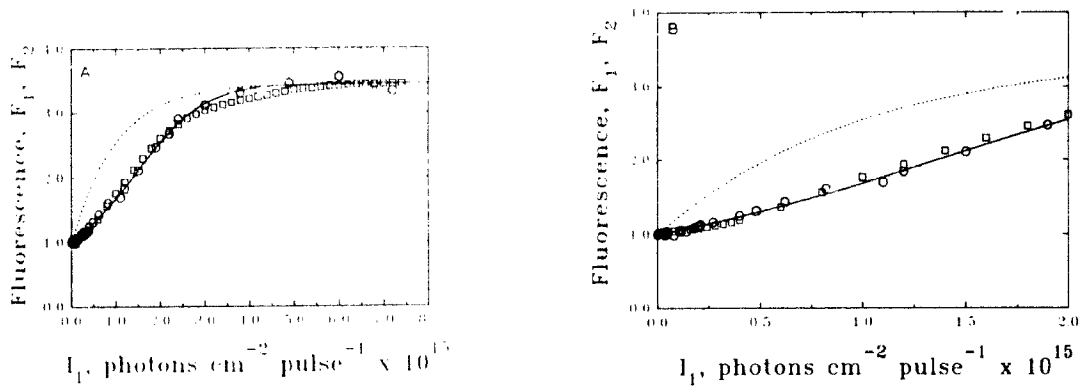

Fig. 4. (A) F_2 (○) variable fluorescence yield as a function of fluence of the actinic pulse, generated by a 2 μs xenon probe flash incident on the sample (10 μM DCMU) after a time delay (Δt) of 18 ms following 13 ms helium neon laser pump flashes of variable fluences, I_1. The solid line (———) represents the best fit of Eqn. 4 to the experimental data points ($p = 0.612$, $\sigma = 5.77 \cdot 10^{-16}$ cm^2, $R = 3.45$). The dotted line (· · · · · ·) represents an exponential rise curve (Eqn. 4, $p = 0.0$, $R = 3.45$, $\sigma = 1.0 \cdot 10^{-15}$ cm^2); the value for σ was selected so that this calculated curve would reach the F_M level at the same fluence as the experimental data. $F_1(t)$ (□), variable fluorescence measured at various time points during the single, high fluence pump flash ($I_1 = 7.2 \cdot 10^{15}$ photons cm^{-2} pulse^{-1}, $t_1 = 13$ ms). Maximum fluorescence induction ratio, $R_\infty = 3.44$. (B) The data in the low fluence region are shown on an expanded scale.

methods should not influence the shapes of the induction curves according to these equations [15]. The results shown in Fig. 4 demonstrate that this assumption is valid for the millisecond time range. The fluorescence induction curves were measured, using the same sample, by two methods in which the reaction centers were closed by a 13 ms He-Ne laser pulse. In Method A, 13 ms actinic pulses of various fluences (I_1) were followed by 2 μs xenon probe flashes ($\Delta t = 18$ ms); the data points (open circles) represent the probe-generated fluorescence yield (F_2); the different P_1 flash fluence rates were obtained by means of neutral density filters. In Method B, the instantaneous fluorescence yield, $F_1(t)$, was measured during the time-course of the single 13 ms actinic flash (open squares, $F_1(t)$ plotted as a function of the fluence $I_1(t)$ evaluated at the time point t)); the fluence rate of this pulse ($5.4 \cdot 10^{17}$ photons cm^{-2} s^{-1} pulse^{-1}) was sufficiently high so that the F_M value was reached well before the end of the 13 ms illumination. This latter

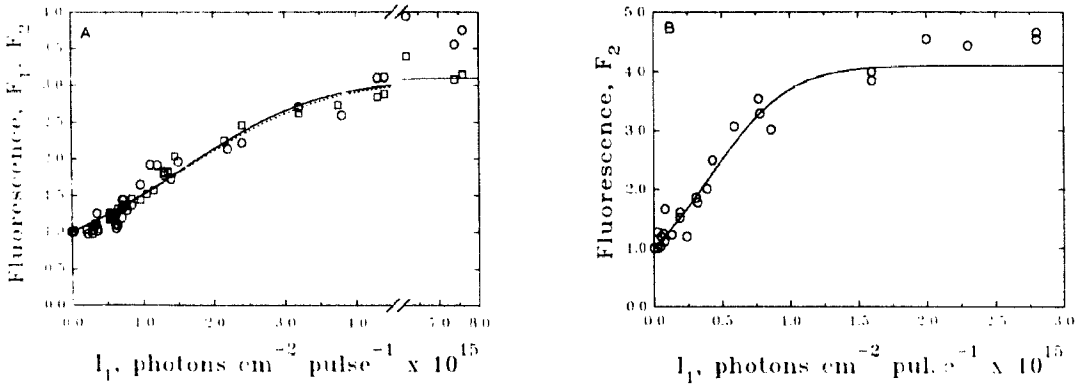

Fig. 5. (A) F_2 (○), variable fluorescence as a function of fluence of the actinic pulse, generated by a 2 μs xenon probe flash incident on the sample (10 μM) with a time delay $\Delta t = 5$ ms after the actinic helium neon laser flashes. The fluence, I_1, of the helium neon laser pulse was varied by changing the duration, t_1, of the pump flash from 5 ms to 140 ms, while keeping the pump flash fluence rate constant. $F_1(t_1)$ (□), variable fluorescence yield determined at the end of each pump flash. The lines represent best fits of Eqn. 4 to the experimental data points using $R = 3.1$. (———).... Theoretical fit to the F_2 data ($p = 0.577$, $\sigma = 4.93 \cdot 10^{-16}$ cm^2). (· · · · · ·) Theoretical fit to the F_1 data (— — —) ($p = 0.564$, $\sigma = 4.78 \cdot 10^{-16}$ cm^2). (B) Variable fluorescence yield generated by a 2 μs xenon probe flash incident on the sample 5 ms after 136 ms helium neon laser flashes of variable fluence. The pump flash fluence, I_1, was varied by decreasing the fluence rate of the pump flashes with neutral density filters, while keeping the duration, t_1, constant. The solid line represents a fit of Eqn. 4 to the F_2 data points ($p = 0.558$, $\sigma = 1.76 \cdot 10^{-15}$ cm^2, $R = 4.1$).

experiment corresponds to the conventional steady-state illumination method of recording fluorescence induction curves. In both cases, DCMU (10 μM) was present to allow for the large separation in time between the actinic and probe pulses.

The induction ratios (3.45), were the same in both experiments, and the shapes of the fluorescence induction curves are identical within experimental error in the high fluence (Fig. 4A) and low-fluence regions (Fig. 4B).

The solid line in Fig. 4A represents the best fit of Eqn. 4 to the experimental data points ($p = 0.612$ and $\sigma = 5.77 \cdot 10^{-16}$ cm^2). For comparison, the dashed line represents an exponential-rise curve (Eqn. 4, with $p = 0$). Both the values for R and p measured by the probe flash, are typical of curves produced using steady-state illumination on milliseconds to seconds time-scales. We thus conclude that the use of 2 μs probe flashes is valid for determining the yield of the variable fluorescence.

To further confirm the validity of this conclusion, two other, similar experiments were performed in which the fluence of the actinic He-Ne laser pulses was varied, but a 2 μs Xe flash was utilized to measure F_v (10 μM DCMU); the separation between the actinic and probe pulses was the same in both types of experiments ($\Delta t = 5$ ms). In Method C, the fluence rate of the He-Ne laser pulses was held constant, while the duration (t_1) of the pulses was varied incrementally from 5 ms to 140 ms to achieve different actinic fluences I_1. In Method D, the duration (t_1) of illumination was held constant, and the fluence (I_1) was varied by using neutral density filters to decrease the fluence rate in increments. The data in these experiments show a relatively poorer signal/noise ratio, because the time constraints imposed by the light sources and triggering system resulted in fewer measurements per data point. For the data in Fig. 5, generally 5–10 measurements per data point were made, whereas in all other experiments there were 50–300 measurements per data point.

The results of the experiments performed according to Method C are shown in Fig. 5A. In addition to measuring the variable fluorescence yield with the 2 μs probe flash (F_2,○), the variable fluorescence yield was also evaluated at the very end of the P_1 actinic pulse ($F_1(t_1)$,□). These F_1 and F_2 data points are nearly superimposable, except for the high fluence region, where the signal/noise ratio is poor. The higher values of F_2 in this region are due to the well-known variability of F_M, especially within the first hour after preparation (see above); the F_2 high-fluence data points (○) in Fig. 5A are examples of this effect, since these measurements were made at the beginning of this lengthy experiment.

Best fits of Eqn. 4 to the data points, using $F_M/F_o = 3.1$, is also shown in Fig. 5A ($p = 0.577$ and $\sigma = 4.93 \cdot 10^{-16}$ cm^2). It is clear that the variable fluorescence measured by either the F_2 or F_1 methods are the same within experimental error.

Results of the Method D experiment are shown in Fig. 5B. The duration of the actinic flash in this experiment was 136 ms, and was kept constant at all fluences. The probe-generated fluorescence (F_2, circle) is plotted at each measured fluence (I_1). Again, the high fluence F_2 measurements were made at the start of the experiment. A value of $F_M/F_o = 4.1$ was used to fit the data points ($p = 0.564$ and $\sigma = 1.76 \cdot 10^{-15}$ cm^2).

Both Method C (which simulates steady-state conditions) and Method D (which simulates pump-probe conditions) on longer time-scales, result in sigmoidal fluorescence induction curves, with $p > 0.56$ and $R > 3$. These results confirm the conclusion drawn from the previous experiment (Fig. 4): on millisecond time-scales, sigmoidal curves with $R > 3$ are observed, regardless of the method used to measure the variable fluorescence.

The value of σ deduced from the fitting of Eqn. 4 to the fluorescence induction data is $\approx 5 \cdot 10^{-16}$ cm^2 in Figs. 4 and 5A, and about 3-times larger in Fig. 5B; these apparent variations in the cross-sections are most likely due to differences in the spinach chloroplasts because these experiments were carried out on different days with different spinach samples.

3.5. Possible effects of DCMU

The redox state of PS II reaction centers depends, in part, on their interactions with the plastoquinone pool. The secondary acceptor, Q_B, a plastoquinone, temporarily binds to PS II; after charge separation in which the primary acceptor Q_A is reduced, Q_A^- is oxidized by Q_B with a half-time of ~200 μs [31]. While it is bound to the PS II complex, Q_B undergoes two successive reduction steps, before it is released. It has been shown that the acceptor kinetics dominate the PS II fluorescence during the time range ~50 μs to ~10 ms, and that during this time-range, oscillations in the fluorescence yield are observed with a two-state periodicity, due to the difference in the reduction rates of Q_B and Q_B^- by Q_A^- [31–34].

The photosynthetic inhibitor, DCMU, preferentially binds to PS II at the Q_B binding site. Therefore, in the presence of 10 μM DCMU, Q_B does not bind to PS II and reoxidation of Q_A^- is prevented. Steady-state-illuminated fluorescence induction curves are traditionally observed in the presence of the inhibitor DCMU in order to prevent re-oxidation of Q_A^- during the experiment. The pump-probe technique allows F_V to be measured in the absence of DCMU, if the time between the onset of the pump flash (P_1) and the arrival of the probe flash (P_2) is $\leqq 100$ μs, since re-oxidation of Q_A^- is still quite limited ~50–100 μs after the initial charge separation. It is possible that, in the absence of DCMU, the presence of the temporarily

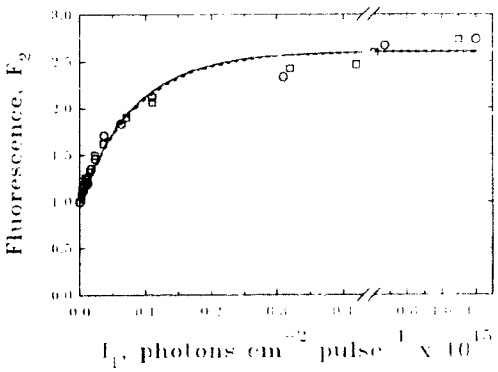

Fig. 6. Fluorescence induction curves (F_2) as a function of the fluence of actinic pulses, generated by a 2 μs xenon probe flash (time delay $\Delta t = 30$ μs) in the presence (□) and absence (○) of 10 μM DCMU. The pump flash was a 300 ps, 337 nm, nitrogen laser flash. The theoretical curves represent the best fits of Eqn. 4 to the experimental data points. (———).... no DCMU, $R = 2.6$, $p = 0.0$, $\sigma = 1.22 \cdot 10^{-14}$ cm^2; (------).... 10 μM DCMU, $p = 0.0$, $\sigma = 1.18 \cdot 10^{-14}$ cm^{-2}.

bound secondary acceptor, Q_B, may affect the shape of the fluorescence induction curves.

In order to eliminate DCMU as a causative factor in the appearance of sigmoidicity and $R > 3.0$, we repeated the pump-probe experiment using a 300 ps, 337 nm pump flash and $\Delta t = 30$ μs, in the presence (Fig. 6, squares) and in the absence (Fig. 6, circles) of 10 μM DCMU. The data shown in Fig. 6 were collected on the same day, using samples prepared from the same pellet of chloroplasts. Both sets of data were normalized to unity at their F_0 levels, and both curves display the same shape, and the same induction ratios ($R = 2.6$). It should be noted that the two curves in Fig. 6 are identical in the range $F_0 \leqq F_2 \leqq F_M$.

The solid and dashed lines in Fig. 6 represent the best fit of Eqn. 4 to the experimental data measured in the absence and presence of 10 μM DCMU, respectively. The values returned by computer analysis were: $p = 0.0$, $\sigma = 1.22 \cdot 10^{-14}$ cm^2 (no DCMU); and $p = 0.0$, $\sigma = 1.18 \cdot 10^{-14}$ cm^2 (10 μM DCMU). Thus, DCMU does not affect the shapes of the fluorescence induction curves in these pump-probe experiments.

3.6. Possible effects of S-states on fluorescence induction curves

The redox state of the OEC-complex is known to affect the fluorescence yields. The OEC-complex reduces the PS II reaction center complex once after each charge separation, and cycles through four redox states (S-states) for each molecule of O_2 that is released [35–37]. The rate constants for the S-state kinetics are generally believed to be of the order of tens to hundreds of microseconds [38]. Dekker et al. measured the half-times for the reactions, $S_i \rightarrow S_{i+1}$ ($i = 0,1,2,3$), in dark-adapted, oxygen-evolving PS II preparations in the presence of an electron acceptor (2,5-dichloro-*p*-benzoquinone), and reported values of 30 μs, 110 μs, 350 μs, and 1300 μs, respectively [39]. The states S_0 and S_1 are stable in the dark, whereas the states S_2 and S_3 tend to decay to S_1, with time constants on the order of 40 s [40]. Thus, for dark-adapted chloroplasts, the S-state composition is believed to be ~ 25% S_0 and ~ 75% S_1.

It has been shown that small, predictable oscillations in the amplitude of the fluorescence yield (± 10%) occur as the redox state (S-state) of the water-splitting complex is changed. Using a series of saturating actinic flashes, spaced 1 s apart, Delosme showed that the fluorescence yield generated by a time-delayed probe flash showed small (± 10%) oscillations in amplitude, which recurred with a characteristic four-state periodicity [41,42]. This was true when the fluorescence was probed at < 20 μs (F_M), as well as at nearly 1 s (F_0), after the actinic flash, although the oscillatory patterns were different for F_M and F_0. These oscillations were damped out after ~ 16 flashes, due to a mixing of the S-states which arises from a small fraction of the S-complexes undergoing two transitions during a single flash, and another small fraction undergoing no transition during the flash.

For illumination periods ≧ several milliseconds, the S-state composition of the system is expected to be well-mixed. In contrast, the S-state composition during a typical pump-probe experiment should be relatively homogeneous, if a submicrosecond actinic flash is used. We therefore designed a series of pump-probe experiments to investigate the consequences of a heterogeneous S-state mixture on the shape and amplitude of the fluorescence induction curves produced with submicrosecond pump flashes. The basic conditions used to generate the results shown in Fig.3B were retained. That is, a 300 ps, 337 nm pump flash was followed by a 2 μs xenon probe flash, with $\Delta t = 30$ μs. No DCMU was present. In these experiments a series of 2, 3, 4 and 15 P_1 pump flashes were employed to close the PS II reaction centers. These flashes were equal in fluence and were spaced 1 s apart. In each case, the results were compared with results produced using one pump flash during the same experiment. The results are listed in Table I (a more detailed description of these results is available elsewhere [16]). In all cases, sigmoidicity was absent, and fitting Eqn. 4 to the experimental data yielded values of $p = 0.0$. In addition, the induction ratios ranged from $R = 2.35$ to 2.65, as was typical for the pump-probe curves measured with 300 ps, 337 nm pump flashes. These data indicate that the mixing of the S-states (which can be assumed to occur in steady-state experiments) is not responsible for the appearance of sigmoidicity.

TABLE I

Characteristics of pump-probe fluorescence induction curves, using multiple pump flashes to mix the S-states

A series of 300 ps, 337 nm pump flashes, spaced 1 s apart was followed by a 2 μs xenon probe flash. The time delay between the final pump flash and the probe was 30 μs. NoP_1 = number of pump flashes in the series. $R = F_M / F_o$, as measured by the probe flash. p = connectivity parameter (Eqn. 2). σ = absorption cross-section (Eqn. 4). χ^2, see Eqn. 5.

Experiment	No. P_1	R	p	σ (cm^2)	χ^2
1	1	2.35	0.0	$1.45 \cdot 10^{-14}$	0.00559
	2	2.35	0.0	$1.36 \cdot 10^{-14}$	0.0116
	3	2.35	0.0	$1.23 \cdot 10^{-14}$	0.00831
2	1	2.65	0.0	$7.62 \cdot 10^{-15}$	0.0297
	4	2.65	0.0	$9.69 \cdot 10^{-15}$	0.0120
3	1	2.25	0.0	$1.34 \cdot 10^{-14}$	0.00956
	15	2.50	0.0	$1.05 \cdot 10^{-14}$	0.0193

3.7. The effects of pump flash duration on sigmoidicity

The results shown in Figs. 2–6 suggest that the time-scales of the experiments may represent an important factor in determining the sigmoidicity of fluorescence induction curves. The pump-probe experiments using submicrosecond pump flashes are characterized by values of the parameters $p \leqq 0.3$, and $R < 3.0$. In contrast, the fluorescence induction curves measured with actinic pulse durations $t_1 \geqq 13$ ms are sigmoidal, with $p > 0.5$ and $R > 3$. To investigate the effect of the pump flash duration, we conducted a set of pump-probe experiments using available xenon pump flashes with significantly different pulse durations in the microsecond range. In these experiments, the absolute energy of the actinic flashes could not be determined accurately because wide-bandpass optical filters were used; the fluence is thus reported in relative units.

The variable fluorescence, F_2, generated with a 2 μs pump flash, followed by a 50 μs xenon probe flash, with $\Delta t = 900$ ms, is shown in Fig. 7A. The solid line represents Eqn. 4 with $p = 0.284$, and $F_M = 2.6$. The shapes of the plots in Figs. 3A and 7A are very similar to one another, because of the similarity of the pump-pulse durations (t_1), which are 0.7 μs and 2.0 μs, respectively. The values of p determined by the least-squares fit are ≈ 0.3. The fluorescence induction ratios R are < 3. It is interesting to note that the duration of the probe flash (e.g., 50 μs in Fig. 7A) does not appear to influence the shapes or amplitudes of the induction curve. This result is expected, since the fluence of the probe flash is kept as low as possible during these experiments.

In this set of experiments, the time delay, Δt, was increased to 500–900 ms (in the presence of 10 μM DCMU), in order to determine whether increasing the dark time prior to the probe flash would give rise to sigmoidicity and $R > 3$. Inspection of Figs. 3A and 7A also shows that increasing the time delay (Δt) between P_1 and P_2 does not result in sigmoidicity. The fluences of both the 50 μs and the 2 μs probe pulses in the experiments of Figs. 7A and 7B, respectively, were adjusted so that they elicited fluorescence signals of equal intensities; their fluences were therefore the same.

The differences in the degrees of sigmoidicities obtained with the short (microsecond or submicrosecond) and the millisecond actinic pulses, suggest that the duration of the actinic light pulses plays an important

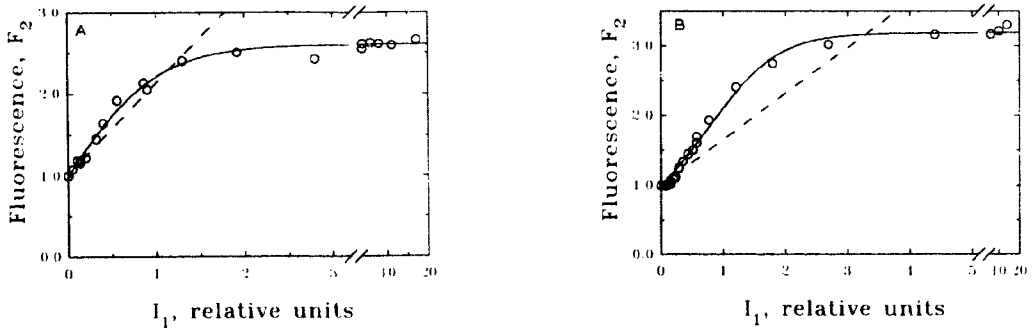

Fig. 7. Variable fluorescence yield (F_2(○)) measured by xenon probe flashes, as a function of the fluence (I_1) of actinic pulses (in relative units, see text). (A) Actinic flash: 2 μs xenon flash; probe pulse: 50 μs xenon probe flash, $\Delta t = 900$ ms, 10 μM DCMU. The solid line represents a best fit of Eqn. 4 to the experimental data using $R = 2.6$, $p = 0.284$, and $\sigma = 1.32$ (relative units). (B) Actinic flash: 50 μs xenon flash; probe pulse: 2 μs xenon flash, $\Delta t = 500$ ms, 10 μM DCMU. These two xenon flashes are the same as those used to generate the data in (A), except that the pump and the probe flashes have been interchanged. The solid line represents a best fit of Eqn. 4 to the data points with $R = 3.19$, $p = 0.543$, and $\sigma = 0.76$ (relative units). The dashed lines in (A) and (B) are straight-line linear regression fits of the data points in the initial portion of the induction curves ($F_2 = 1.0$–1.3). The greater the deviations of the subsequent ($F_2 > 1.3$) data points, the greater the degree of sigmoidicity (see text).

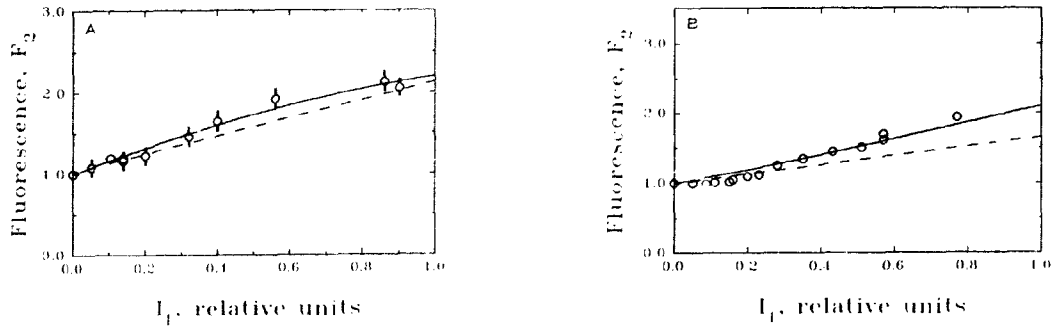

Fig. 8. Low fluence region of fluorescence induction curves shown in (A) Fig. 7A and (B) Fig. 7B.

role in this effect. To test the assumption that it is the duration (t_1) of the pump flash that determines the shape and amplitude of the fluorescence induction curves, we exchanged the light sources (P_1 and P_2) which were used to generate the results in Fig.7A. Fig. 7B shows the results obtained using a 50 μs xenon pump flash which was followed by a 2 μs probe flash, with Δt = 500 ms. This curve is clearly sigmoidal in shape, and the fluorescence induction ratio is higher (R = 3.2). The solid line, generated by means of Eqn. 4 with p = 0.543, is also shown. The dashed lines in Fig. 7 are straight-line, linear regression fits to the experimental data points in the initial portion of the fluorescence induction curve (F_2 = 1.0–1.25); these initial low-fluence regions are shown in the expanded plots of the data in Figs. 8A and 8B. In a purely exponential fluorescence induction curve, all of the higher F_2 points (> 1.3) should lie below the extrapolated dashed line.

TABLE II

Characteristics of fluorescence induction curves, measured with different pump flash durations (t_1) [a]

Δt = time delay between pump and probe flashes. $R = F_M / F_0$, as measured by the probe flash. $R_{ss} = F_M / F_0$, as measured by steady-state illumination beam (≥ 13 ms) on the same sample. p = connectivity parameter which gives best fit of the experimental data (F_2) to Eq. 2.

t_1	Δt	R	R_{ss}	p	χ^2
300 ps (337 nm)	30 μs	2.5 [b]	–	0.0 [b]	0.00341
300 ps (337 nm) [c]	30 μs	2.0	4.4	–	–
700 ns (650 nm)	100 μs	1.7	–	0.26	0.000434
1.2 μs (385–555 nm)	900 ms	3.0	–	0.49	0.00695
2.0 μs (385–555 nm) [a]	900 ms	2.6	3.1	0.29	0.00415
50 μs (385–555 nm)	500 ms	3.2	3.4	0.54	0.00627
13 ms (633 ns)	18 ms	3.4	3.4	0.61	0.00202
136 ms (633 nm)	5 ms	4.1	4.5	0.56	0.0766
140 ms (633 nm)	5 ms	3.1	3.3	0.58	0.0631

Probe flash: 2 μs xenon flash in all cases, except:
[a] 50 μs xenon flash.
[b] Mean values of three experiments;
[c] Mean values of two experiments. Other values represent the results of typical experiments.

In sigmoidal induction curves, all of the higher F_2 points should lie above this line. It is evident that the positive deviations from the dashed straight line of the experimental points in Fig. 7B are significantly higher than they are in Fig. 7A. Thus, the degree of sigmoidicity is significantly higher in the case of the 50 μs than in the case of the 2 μs actinic pulse.

We conclude that the threshold for the appearance of sigmoidity and $R > 3$, necessitates actinic pulse durations in the microsecond range (t_1 in the range of ≈ 2 – 50 μs).

3.8. Correlation between t_1 and R

There is a crude correlation between the duration of the actinic pump flashes (t_1) and the induction ratio (R) (Table II): as the lengths of the actinic flashes is increased, there is also a general increase in the F_M/F_0 ratio, as well as in the degree of sigmoidicity as expressed by the calculated parameter p. The values of R were determined in these pump-probe experiments utilizing a probe flash P_2 incident on the sample some time interval Δt after the end of the actinic flash. In some cases, the values of R_{ss} were also determined for exactly the same samples using a 13 or 140 ms (632.8 nm) steady-state He-Ne laser beam. In the case of the short actinic flashes, our results correlate well with those reported by Mauzerall [12] who employed a 7 ns, 337 nm pump flash followed by a xenon probe flash, with Δt = 30 μs, and observed an R value of 2.4.

4. Discussion

4.1. Variability of shapes of fluorescence induction curves

Exponential fluorescence induction kinetics have been predicted or are observed using: (1) steady-state illumination under certain conditions, (2) low values of R (R < 1.5, or p < 0.33 [43]), (3) low temperature [44], (4) low magnesium ion concentrations [45], (4) presence of external quenchers (300 μM *m*-dinitrobenzene (DNB)) [3], and (5) pre-illumination under certain conditions [4,46]. In each of these cases, the absence of

sigmoidicity could be attributed to a decrease in connectivity caused by the particular experimental conditions. In the case of pump-probe fluorescence induction curves employing sub-microsecond actinic flashes, the exponential shapes of the fluorescence induction curves cannot be simply attributed to a lack of connectivity; the same chloroplasts exhibit sigmoidal fluorescence induction curves when illuminated on longer time-scales.

Furthermore, regardless of the mechanisms of closure of PS II reaction centers, the variable fluorescence generated by the weak xenon probe flashes should itself yield sigmoidal induction curves even if q is exponentially dependent on the fluence of the actinic pulses ($p = 0$, Eqn. 2); this latter condition could occur for example, when actinic pulses of less than ≈ 50 ns duration are employed since the presence of P^+ quenchers would tend to diminish interunit transfer (section 3.1). Eqn. 2, based on the standard explanation of connectivity between PS II units, predicts that the dependence of the variable fluorescence on q should be non-linear; this prediction should apply to the probe-flash detected fluorescence as well [21]. Since, exponentially shaped induction curves are observed with short actinic pulses, Eqn. 2 does not seem appropriate for the interpretation of these experiments [21].

We have shown here that in pump-probe experiments, the shapes and the amplitudes of fluorescence induction plots depend on the duration, t_1, of the actinic excitation pulses. We have demonstrated that sigmoidal character of induction curves, whenever present, can indeed be revealed by weak, 2 μs xenon probe flashes; thus the probe-flash technique cannot account for the observation of exponential induction curves when submicrosecond actinic flashes are employed, since the shapes of the curves are clearly sigmoidal when the length of the actinic pulses exceeds ≈ 50 μs.

The results summarized in Table II indicate that when the duration of the actinic pulses $t_1 \leqq 2$ μs, the fluorescence induction ratio, R, is < 3.0, and the value of p obtained by a least-squares fit of Eqn. 4 is $\leqq 0.5$, and generally less than 0.3; occasionally, relatively high values of p (≈ 0.5) are observed when microsecond duration actinic flashes are employed (see the 1 μs actinic flash result in Table II). It should be noted that variabilities in the p values ($p = 0.4$–0.65) were also reported by Joliot and Joliot [1] in their steady-state fluorescence induction experiments.

When $t_1 \geqq 50$ μs, $R > 3.0$, the values of p recovered from fits of Eqn. 4 to the data are greater than 0.5; these values are characteristic of sigmoidal fluorescence induction curves [1].

To summarize, the critical duration t_1 of the actinic pulses above which sigmoidicity becomes apparent, appears to lie in the range of ≈ 2–50 μs. This is evident from the experimental results shown in Figs. 7A and 7B. In these two experiments, all conditions were the same except that the 2 μs and 50 μs pump and probe xenon flashes were interchanged. In Fig. 7A the actinic pulse was the 2 μs flash, while the 50 μs xenon flash served as the probe pulse; the fluorescence induction curve is clearly non-sigmoidal with $p = 0.264$, while R is only 2.6. In Fig. 7B, the actinic flash is 50 μs long, while the 2 μs xenon flash served as the probe flash; the induction curve is clearly sigmoidal with $p > 0.5$ and $R > 3.0$. This difference is solely due to an increase in t_1 from 2 to 50 μs. The parameters R and p appear to be unaffected by the presence or absence of DCMU (Fig 5), the overall S-state composition (Table I), or the length of the delay time Δt between the actinic and probe pulses (Table II).

The fact that the redox states of both the OEC-complex and the secondary acceptor, Q_B, can influence the fluorescence yield of PS II, suggests that either of these species may be linked to the appearance of sigmoidicity, and R factors greater than 3. However, our results do not support this hypothesis. The rate constants generally cited for the oxidation of Q_A^- by Q_B are longer than the critical time $t_1 \approx 2$–50 μs we observe for the appearance of sigmoidicity. First, the half-times for the oxidation of Q_A^- are on the order of ~ 200 μs [31]. This indicates that the shapes of fluorescence induction curves are not affected by whether or not Q_B is bound to the reaction center complex. Second, in regard to the OEC-complex, the half-times for the turn-over of the S-states are $\geqq 350$ μs, except for the reactions, $S_0 \rightarrow S_1$ ($\tau \approx 30$ μs) and $S_1 \rightarrow S_2$ ($\tau \approx 110$ μs) [38]. In view of the similarity between the latter two rate constants and the actinic pulse illumination time t_1 marking the transition from exponential to sigmoidal induction curves, the possible roles of these S-states should be reconsidered in more detail. The S-state composition is predicted to be $\sim 75\%$ S_2 and $\sim 25\%$ S_1 at the arrival of the probe flash (after one saturating actinic flash). Since we used a series of actinic flashes with equal fluences (I_1), rather than saturating flashes prior to P_2, the S-state composition in the low fluence range is somewhat indeterminate. However, in the high fluence range of each experiment, the S-state turnover should approach 100% (except for small fractions of double hits and misses). Therefore, at the very least, an increase in R should have been observed in experiments 1 and 2 (Table I), if any of the individual S-states are linked to the higher induction ratios observed in sigmoidal curves. Also, a similar line of reasoning applied to an interpretation of experiment 3 (Table I), suggests that changes in p and R would be observed when a train of actinic flashes is employed to mix the S-state composition. The fact that neither the connectivity parameter p nor the fluorescence induc-

tion ratio R is sensitive to the number of identical actinic flashes incident on the sample, suggests that the occurrence of mixed S-states does not play a critical role in the appearance of sigmoidicity and large fluorescence induction ratios ($R > 3$).

Possible effects of the pulse-separation, Δt, must also be considered. However, we have observed that increasing Δt values from 30 μs to 500–900 ms (in the presence of DCMU), does not produce sigmoidal induction curves ($p > 0.5$ and $R > 3$), as long as actinic pulse duration $t_1 \leqq 2$ μs (Table II).

4.2 The possible role of triplet excited state quenchers

The lifetimes of carotenoid triplets, which are known to quench the fluorescence of PS II, are ≈ 5 μs [23,24]. However, these triplet quenchers do not play a significant role in the detection of the fluorescence yield probed with the P_2 flash 30 μs or more after the incidence of the actinic flash [16] (see also [30]).

However, during the actinic pulse itself (especially on microsecond time-scales [23,24]), quenching of excitations by carotenoid triplets could, in principle, influence the shapes of fluorescence induction curves. Quenching leads to a decrease in the mean lifetimes of the singlet excitations (reviewed in Ref. 2), and therefore a decreased efficiency of interunit transfer is expected. In turn, low values of p give rise to exponential rather than sigmoidal induction curves (Eqn. 2). The possibility that this effect could account for the lack of sigmoidicity in fluorescence induction curves measured by microsecond actinic pulse-probe double flash techniques has been considered in detail [16,21]. Briefly, within the context of the lake model, the fraction of reaction centers closed by an actinic flash (q) is related to the integrated fluorescence yield measured during the actinic flash (Φ) by the following equation [2,14]:

$$q = 1 - \exp\{-\sigma\phi_1\} \qquad (6)$$

The values of q measured by the probe flash and the value of Φ measured during the actinic flash were compared experimentally [16,21]. The decrease in Φ sets in at actinic pulse fluences almost 10-times greater than the onset of fluorescence induction as measured by the probe flash (≈ 1 μs actinic flash, delay time between the flashes $\Delta t = 100$ μs). Furthermore, the lowered values of Φ due to singlet-triplet quenching did not cause any significant deviations of q from a truly exponential growth curve (i.e. when $\Phi = 1.0$ in Eqn. 6). On the basis of these results, it was concluded that the capture of excitations by PS II reaction centers is much more efficient than singlet-triplet exciton quenching at the relatively low fluences required for closing the PS II reaction centers.

In summary, triplets generated during the actinic pulse do not appear to be effective in changing the shapes of the fluorescence induction curves; the observed fluorescence quenching occurs at higher P_1 pulse fluences when almost all of the RC's are closed [16,21]. Therefore, our results are not inconsistent with the strong quenching of the fluorescence by triplets observed *during* the actinic pulses by Sonneveld et al. [24] and by Breton et al. [23]. In our experiments, the fluorescence is probed by a second pulse, which is incident on the sample *after* the triplets have decayed.

4.3. Possible effects of PS II or reaction center heterogeneity

Several types of PS II heterogeneity have been noted. The growth of the area above the fluorescence induction curve ($\int_0^t (F_M - F(t))dt$) in the presence of DCMU, can be resolved into one fast and one slow-growing component, attributed to PS II_α and PS II_β, respectively [6,7,47,48]. In the smaller PS II_β antenna system [49,50], electron transport does not seem to involve the two-electron-accumulating plastoquinone mechanism [51]. Lavergne [52] found that a fraction of PS II reaction centers are unable to transfer electrons efficiently from Q_B to the plastoquinone pool (non-Q_B centers), and the nature of these less active centers has been investigated [53,54]. The possible relationship between PS II_β, non-Q_B centers, and fluorescence induction kinetics, has been recently discussed by Cao and Govindjee [55]. In steady-state illumination induction kinetics in the absence of herbicides, a very rapid rise from the initial level F_0 to a higher intermediate plateau level F_I (or F_{pl} level, with $F_I/F_0 \approx 1.5$–2 [47,55]) is observed if the time-resolution of the induction experiment is sufficiently high (the O-I-D rise [47,55,56]); as the illumination is continued, the fluorescence rises from the level D to the level P (F_M), which corresponds to the accumulation of electrons on the primary acceptor Q_A due to the reduction of the plastoquinone pool. Melis suggested that the $F_0 \rightarrow F_I$ rise is the variable fluorescence yield controlled by PS II_β [47]. Cao and Govindjee concluded that this rise can be attributed to the reduction of Q_A to Q_A^- in inactive PS II centers, but it is not yet clear whether these can be identified with PS I_β RC's (Ref. 55, see also Ref. 52).

In steady-state experiments, the F_I level is reached at approx. 5–10% of the fluence required to reach F_M. In double-pulse experiments, analogous effects might be expected in the low fluence region of actinic pulses. However, such effects were not observed in our double-pulse induction experiments. In the absence of DCMU, the variable fluorescence yield rises exponentially with the actinic pulse fluence (Fig. 3). Below the P_1 fluence threshold for the onset of induction, the measured fluorescence intensity was linearly proportional to the actinic pulse fluence and the yield (F_0) was constant as the P_1 fluence was lowered by another

factor of 5–10 below this threshold [16]. In the presence of DCMU, effects at low fluences analogous to the O-I-D induction were not observed either; the Fig. 7 values of F_2 measured at low actinic pulse fluences are shown in Fig. 8 as an example.

Since, in the case of the submicrosecond actinic pulses, the fluorescence induction growth is exponential or close to exponential, the presumed 3:1 PS II_α:PS II_β antenna heterogeneity [47] is not evident in these experiments. However, this lack of manifestation of the PS II_α/PS II_β heterogeneity may be due to the difficulties associated with determining bimodal distributions of antenna sizes from double-pulse photosynthetic yield and/or fluorescence induction experiments [57,58].

The shapes of the fluorescence induction curves obtained with actinic pulses > 50 μs in duration (and in the presence of DCMU) are consistent with the PS II_α/PS II_β heterogeneity, because they are sigmoidal in shape and resemble the steady-state illumination induction curves. However, there is no obvious reason why this same heterogeneity in the antenna cross sections should not also manifest itself when shorter actinic pulses are employed. Since only the time-scales of the excitation, but not the fluences are different, these results suggest that other time-dependent effects may be responsible for the changes in shape of the induction curves as the actinic pulse lengths are increased.

4.4. A sequential double-hit model can account for exponential and sigmoidal fluorescence induction curves

The appearance of sigmoidicity ($p > 0.5$) when $t_1 \geq$ 50 μs (Fig. 7C; Table II) suggests that the prerequisite for observing sigmoidicity and $R > 3$ involves the absorption of two excitations by the PS II reaction centers, with an intervening dark-lag time τ_1 [18,21]. This model, which is similar to a double-hit model previously proposed by Lavorel [5], can be summarized as follows:

$$Q_0 \xrightarrow{h\nu_1} Q_1 \xrightarrow{\tau_1^{-1}} Q_2 \xrightarrow{h\nu_2} Q_3 \qquad (7)$$

where Q_0 denotes open PS II reaction centers, while Q_1, Q_2, and Q_3 are states of PS II reaction centers. The variable fluorescence yield is different for each of these three states and is assumed to increase as the PS II reaction centers progress from left to right in Eqn. 6. The overall observed variable fluorescence yield depends on the fractions of PS II reaction centers in each of these three states. The state Q_1 acts as a delay τ_1 for the effective utilization of a second excitation, corresponding to some evolution of the PS II reaction centers from the state Q_1 to the state Q_2. Thus, a second excitation must be absorbed in order to generate the highly fluorescent state Q_3.

According to this model, short actinic pulses of lengths $t_1 < 2$–50 μs, such as the 300 ps and 700 ns duration laser pulses (Fig. 3), cannot advance the PS II reaction centers beyond the state Q_1 even at high fluences corresponding to several hits per reaction centers; when the system is in the state Q_1, the fluorescence yield induction ratio is relatively low ($R < 3$, Table II) with the induction curves exponential or nearly exponential in shape ($p < 0.5$). Actinic illumination on time-scales $t_1 \geq \tau_1$ (in steady-state illumination experiments on millisecond time-scales $t_1 \gg \tau_1$) gives rise to mixtures of Q_1, Q_2, and Q_3 states, each with its own characteristic fluorescence yield. Within the context of this model, as a function of increasing fluence, either exponential or sigmoidal fluorescence induction curves will be observed, depending on the time-scales of the illumination used to close the PS II reaction centers progressively. It has been shown that this model can account for the shapes of the observed pump-probe fluorescence induction curves using reasonable values of the parameters p [18,21].

The nature of the putative intermediate states Q_1, Q_2, and Q_3 cannot be specified on the basis of the simple fluorescence induction curves described here. This question could be investigated by carefully correlating the changes in fluorescence yields measured by double-pulse techniques using actinic pulses of varying lengths, with changes in the concentrations of various known PS II intermediates [59]. Multiple states of PS II with different fluorescence yields (which are formed after one or two hits per reaction center) have been reported [52,60,61]; the lag-time of $\tau_1 \approx 2$–50 μs is in the same time range as the electron transfer time between some of the different S-states [38,62], or the reduction of P^+ by the tyrosine residue YZ under certain conditions [63]. However, the relationships of these phenomena, if any, to the different Q-states (Eqn. 7), remain to be investigated.

4.5. Implications of the sequential hit model

We have shown that the sequential hit model (Eqn. 6) is consistent with the observation of sigmoidal fluorescence induction curves within the context of either a puddle model or a lake (matrix) model of the PSU [18]. The sequential hit model adequately can account for the variabilities of the shapes of fluorescence induction curves as a function of the lengths of the actinic pulses in pump-probe fluorescence induction experiments. Existing models based on Eqns. 2 and 3 cannot account for these observations. The sequential hit model does not contradict the principle of connectivity between different units in PS II; a number of other results suggest that the mean diffusion distances of excitations are limited simply by their lifetimes [2]. An implicit consequence of the sequential hit model is, however, that the shapes of fluorescence induction curves do not

provide any information on the degree of connectivity in PS II. In fact, Ley and Mauzerall [13] have shown that the apparent cross-section of PS II reaction centers does not depend on q, the fraction of closed RCs. The observations of non-sigmoidal and sigmoidal fluorescence induction curves in the same chloroplast samples using illumination pulses of different duration, suggests that the basic phenomena underlying these differences should be investigated further.

Acknowledgements

We would like to acknowledge the assistance of Drs. A. Dobek and J. Deprez in the early experimental stages of this project. This work was supported by a grant from the U.S. Department of Agriculture (Grant No. 88-37262-3859).

References

1 Joliot, A. and Joliot, P. (1964) C.R. Acad. Sci. 13, 4622-4625.
2 Geacintov, N.E. and Breton, J. (1987) CRC Crit. Rev. Plant Sci. 5, 1-44.
3 Lavorel, J. and Joliot, P. (1972) Biophys. J. 12, 815-831.
4 Joliot, P. and Joliot, A. (1977) Biochim. Biophys. Acta 462, 559-574.
5 Lavorel, J. (1972) C.R. Acad. Sci. Paris D 274, 2909-2912.
6 Melis, A. and Homann, P.H. (1976) Photochem. Photobiol. 21, 431-437.
7 Melis, A. and Homann, P.H. (1976) Photochem. Photobiol. 23, 343-350.
8 Bell, D.H. and Hipkins, M.F. (1985) Biochim. Biophys. Acta 807, 255-262.
9 Hodges, M. and Moya, I. (1986) Biochim. Biophys. Acta 849, 193-202.
10 Hodges, M. and Moya, I. (1987) Biochim. Biophys. Acta 892, 42-47.
11 Trissl, H.W., Breton, J., Deprez, J. and Leibl, W. (1987) Biochim. Biophys. Acta 893, 305-319.
12 Mauzerall, D. (1976) Biophys. J. 16, 87-91.
13 Ley, A.C. and Mauzerall, D. (1986) Biochim. Biophys. Acta 808, 192-200.
14 Geacintov, N.E., Paillotin, G., Deprez, J., Dobek, A. and Breton, J. (1984) in Advances in Photosynthesis Research (Sybesma, C., ed.), Vol. 1, pp. 37-40, Martinus Nijhoff, Dordrecht.
15 Geacintov, N.E., Breton, J., France, L., Deprez, J., Dobek, A. and Breton, J. (1987) in Progress in Photosynthesis Research (Biggins, J., ed.), Vol. 1, pp. 107-110, Martinus Nijhoff Publishers, Dordrecht.
16 France, L. (1989) Ph.D. Dissertation, New York University, New York.
17 France, L.L., N.E. Geacintov and J. Breton (1990) in Current Research in Photosynthesis (Baltscheffsky, M., ed.) pp. 467-470, Kluwer Academic Publishers, Dordrecht, The Netherlands.
18 Valkunas, L., Geacintov, N.E., France, L. and Breton, J. (1991) Biophys. J. 59, 397-408.
19 Marquardt, D.W. (1963) J. Soc. Ind. Appl. Math. 11, 431-441.
20 Bevington, P.R. (1969) Data Reduction and Arror Analysis for the Physical Sciences, McGraw-Hill, New York.
21 Valkunas, L., Geacintov, N.E. and France, L. (1991) J. Lumin., submitted.
22 Kramer, M. and Mathis, P. (1980) Biochim. Biophys. Acta 593, 319-329.
23 Breton, J., Geacintov, N.E. and Swenberg, C.E. (1979) Biochim. Biophys. Acta 548, 616-635.
24 Sonneveld, A., Rademaker, H. and Duysens, L.N.M. (1979) Biochim. Biophys. Acta 543, 536-551.
25 Butler, W.L. (1972) Proc. Natl. Acad. Sci. U.S.A. 69, 3420-3422.
26 Deprez, J., Dobek, A., Geacintov, N.E., Paillotin, G. and Breton, J. (1983) Biochim. Biophys. Acta 725, 444-454.
27 Brettel, K. and Schlodder, E. and Witt, H.T. (1984) Biochim. Biophys. Acta 766, 403-415.
28 Van Best, J.A. and Mathis, P. (1978) Biochim. Biophys. Acta 503, 178-188.
29 Schlodder, E., Brettel, K. and Witt, H.T. (1985) Biochim. Biophys. Acta 808, 123-131.
30 Mauzerall, D. (1972) Proc. Natl. Acad. Sci. U.S.A. 69, 1358-1362.
31 Robinson, H. and Crofts, A.R. (1987) in Progress in Photosynthesis Research (Biggins, J., ed.), Vol. II, pp. 429-432, Martinus Nijhoff, Dordrecht.
32 Robinson, H. and Crofts, A.R. (1984) in Advances in Photosynthesis Research (Sybesma, C., ed.) Vol. I, pp. 477-480, Martinus Nijhoff/Dr. W.Junk, The Hague.
33 Bowes, J.M. and Crofts, A.R. (1980) Biochim. Biophys. Acta 590, 373-384.
34 Bouges-Boucquet, B. (1973) Biochim. Biophys. acta 314, 250-256.
35 Kok, B., Forbush, B. and McGloin, M.P. (1970) Photochem. Photobiol.11, 457-475.
36 Joliot, P. and Kok, B. (1975) in Bioenergetics of Photosynthesis (Govindjee, ed.), pp. 387-412, Academic Press, New York.
37 Forbush, B., Kok, B. and McGloin, M.P. (1971) Photochem. Photobiol. 14, 307-321.
38 Gerken, S., Brettel, K., Schlodder, E. and Witt, H.T. (1987) FEBS Lett. 234, 376-380.
39 Dekker, J.P., Plijter, J.J., Ouwenhand, L. and Van Gorkom, H.J. (1984) Biochim. Biophys Acta 767, 176-179.
40 Delrieu, M.-J. (1984) Biochim. Biophys. Acta 767, 304-313.
41 Delosme, R. (1972) in Proceedings of the Second International Congress on Photosynthesis Research (Forti, G., Mordhay, A. and Melandri, A., eds.), pp. 187-195, Dr. W. Junk, The Hague.
42 Delosme, R. (1971) C.R. Acad. Sci. Paris D272, 2828-2831.
43 Paillotin, G. (1976) J. Theor. Biol. 58, 237-252.
44 Amesz, J. and Duysens, L.N.M. (1977) in Topics in Photosynthesis: Primary Processes of Photosynthesis (Barber, J., ed.), Vol. 2, pp. 149-186, Elsevier, Amsterdam.
45 Lavorel, J. and Etienne, A.L. (1977) in Topics in Photosynthesis: Primary Processes of Photosynthesis (Barber, J., ed.), Vol. 2, pp. 203-268, Elsevier, Amsterdam.
46 Joliot, P. and Joliot, A. (1979) Biochim. Biophys. Acta 546, 93-105.
47 Melis, A. (1985) Biochim. Biophys. Acta 808, 334-342.
48 Thielen, A.P.M.G. and van Gorkom, H.J. (1981) Biochim. Biophys. Acta 635, 111-120.
49 Melis, A. and Homann, P.H. (1978) Arch. Biochem. Biophys. 190, 523-530.
50 Melis, A. and Duysens, L.N.M. (1979) Photochem. Photobiol. 29, 373-382.
51 Thielen, A.P.G.M. and Van Gorkom, H.J. (1981) FEBS Lett. 129, 205-209.
52 Lavergne, J. (1982) Photobiochem. Photobiophys. 3, 273-285.
53 Graan, T. and Ort, D.R. (1986) Biochim. Biophys. Acta 852, 320-330.
54 Chylla, R.A., Garab, G. and Whitmarsh, J. (1987) Biochim. Biophys. Acta 894, 562-571.
55 Cao, J. and Govindjee (1990) Biochim. Biophys. Acta 1015, 180-188.
56 Forbush, B. and Kok, B. (1968) Biochim. Biophys. Acta 162, 243-253.
57 Ley, A.C. and Mauzerall, D. (1982) Biochim. Biophys. Acta 680, 95-106.

58 Mauzerall, D. and Greenbaum, N.L. (1989) Biochim. Biophys. Acta 974, 119–140.5
59 Melis, A. and Schreiber, U. (1979) Biochim. Biophys. Acta 547, 47–57.
60 Joliot, P. and Joliot, A. (1981) FEBS Lett. 134, 155–160.
61 Crofts, A.R. and Wraight, C.A. (1983) Biochim. Biophys. Acta 726, 149–185.
62 Saygin, Ö. and Witt, H.T. (1987) Biochim. Biophys. Acta 893, 452–469.
63 Hoganson, C.W., Casey, P.A. and Hansson, O. (1991) Biochim. Biophys. Acta 1057, 399–406.